



Shelf-Sourced Methane in Surface Seawater at the Eurasian Continental Slope (Arctic Ocean)

Elena Vinogradova^{1*}, Ellen Damm², Andrey V. Pnyushkov^{3,4}, Thomas Krumpen⁵ and Vladimir V. Ivanov^{6,7}

¹Shirshov Institute of Oceanology, Russian Academy of Science, Moscow, Russia, ²Permafrost Research Section, Alfred Wegener Institute for Polar and Marine Research, Potsdam, Germany, ³International Arctic Research Center, University of Alaska Fairbanks, Fairbanks, AK, United States, ⁴Global Institution for Collaborative Research and Education, Hokkaido University, Sapporo, Japan, ⁵Sea ice physics Research Section, Alfred Wegener Institute for Polar and Marine Research, Bremerhaven, Germany, ⁶Lomonosov Moscow State University, Faculty of Geography, Oceanology Department, Moscow, Russia, ⁷Arctic and Antarctic Research Institute, St Petersburg, Russia

OPEN ACCESS

Edited by:

Daniel F. McGinnis,
Université de Genève, Switzerland

Reviewed by:

Terry Whitledge,
Retired, Fairbanks, AK, United States
Haiyan Jin,
Ministry of Natural Resources, China

*Correspondence:

Elena Vinogradova
vinogradova@ocean.ru

Specialty section:

This article was submitted to
Biogeochemical Dynamics,
a section of the journal
Frontiers in Environmental Science

Received: 08 November 2021

Accepted: 12 January 2022

Published: 28 January 2022

Citation:

Vinogradova E, Damm E,
Pnyushkov AV, Krumpen T and
Ivanov VV (2022) Shelf-Sourced
Methane in Surface Seawater at the
Eurasian Continental Slope
(Arctic Ocean).
Front. Environ. Sci. 10:811375.
doi: 10.3389/fenvs.2022.811375

This study traces the pathways of dissolved methane at the Eurasian continental slope (ECS) and the Siberian shelf break based on data collected during the NABOS-II expedition in August-September, 2013. We focus on the sea ice-ocean interface during seasonal strong ice melt. Our analysis reveals a patchy pattern of methane supersaturation related to the atmospheric equilibrium. We argue that sea ice transports methane from the shelf and that ice melt is the process that causes the heterogeneous pattern of methane saturation in the Polar Mixed Layer (PML). We calculate the solubility capacity and find that seasonal warming of the PML reduces the CH₄ storage capacity and contributes to methane supersaturation and potential sea-air flux in summer. Cooling in autumn enhances the solubility capacity in the PML once again. The shifts in the solubility capacity indicate the buffering capacity for seasonal storage of atmospheric and marine methane in the PML. We discuss specific pathways for marine methane and the storage capacity of the PML on the ECS as a sink/source for atmospheric methane and methane sources from the Siberian shelf. The potential sea-air flux of methane is calculated and intrusions of methane plumes from the PML into the Cold Halocline Layer are described.

Keywords: methane plumes, polar mixed layer, Eurasian continental slope, sea ice, shelf-basin interaction

1 INTRODUCTION

The Arctic holds large natural sources of methane (CH₄), especially the Siberian shelf, which is considered as potential sources of this greenhouse gas for the atmosphere. The release of CH₄ from these shallow shelf seas threaten to enhance the current Arctic amplification of global warming (IPCC, 2019). Indeed, warmer seawater as a positive feedback on the climate is discussed to displace gas hydrate stability zones and increase the thawing of subsea permafrost, which acts as a physical barrier to ascending gas (Reagan and Moridis, 2008; Shakhova et al., 2019). Recent acoustic surveys on shelves and along continental slopes revealed significant CH₄ emissions, triggered by an increasing number of submarine gas seepages (Westbrook et al., 2009; Baranov et al., 2020; Chuvilin et al., 2020). These assessments of potential CH₄ release mainly focused on the changes in the submarine CH₄ storage system (Shakhova et al., 2010, Shakhova et al., 2014;

Berchet et al., 2016). Based on these methodological approaches, bottom-up flux CH_4 estimations are strongly imbalanced related to top-down flux estimations (AMAP, 2015), revealing that either the release at the submarine-marine interface or the sea-air CH_4 fluxes is overestimated.

Actually, calculations based on the level of CH_4 supersaturation in surface water related to the atmospheric equilibrium disregard the effects of sea ice and the water transformations coupled to the sea ice cycle on the pathways of CH_4 (Damm et al., 2018). According to recent studies, the transport of shelf-sourced CH_4 by sea ice is a driving mechanism causing the patchy appearance of CH_4 excess in surface waters detected in different Arctic regions (Damm et al., 2015, Damm et al., 2018; Verdugo et al., 2021). Consequently, an assessment of the current sink capacities of certain regions and water masses in the Arctic Ocean is urgently needed to better simulate future climate scenarios.

In the last few decades, Arctic sea ice has sharply declined (Screen and Simmonds, 2010). The longer sea ice-free seasons (Markus et al., 2009; Günther et al., 2015) will have significant consequences for the CH_4 cycle, while the elongated period for a potential net sea-air exchange is just one possibility. Intensive sea ice melt causes an increasing contribution of fresh water in surface waters that dilutes the CH_4 excess. Eventually, warming will amplify the water stratification, and restrict CH_4 fluxes into the atmosphere. Water stratification is known to favor lateral CH_4 transport, which in turn enables CH_4 oxidation in the water column (Mau et al., 2013; Gentz et al., 2014; Myhre et al., 2016; Mau et al., 2017; Silyakova et al., 2020; Damm et al., 2021).

Moreover, changes of temperature and salinity in surface water, controlling the solubility and eventually the storage capacity for CH_4 , needs to be considered in assessments of the current CH_4 budget. The Eurasian continental slope (ECS) is a key Arctic region to study this complexity of marine CH_4 pathways and the potential sink capacity of Arctic surface water. The surface water at the ECS comprises the Polar Mixed Layer (PML) on top and the salinity-stratified Cold Halocline Layer (CHL) underneath. In summer, the PML is formed by sea ice melt and Siberian River runoff (Rudels et al., 1996). In winter, ice formation in leads and polynyas alters the characteristics of the PML (Dmitrenko et al., 2009; Krumpfen et al., 2011; Iwamoto et al., 2014). The CHL is formed via interaction between inflowing Atlantic water and sea ice (Rudels et al., 2004). The CHL remains close to the Siberian continental slope, receives inflows from surrounding shelves, and is additionally modified through mixing with the PML (Alkire et al., 2017). Both water masses link the shallow shelf with the ECS and highlight the role of the shelf-basin exchange for the validation of the CH_4 sink capacity.

In this study, we provide a first assessment of the seasonal storage capacity of the PML on the ECS. Based on data collected along cross-slope sections in late summer 2013 we point to the seasonal buffer capacity of the PML, which might influence the CH_4 flux. We discuss the ability of the ECS as a sink for CH_4 under the conditions of current sea ice retreat. Further, we describe the formation of CH_4 plumes in the sea ice-influenced PML during the period of pronounced seasonal ice

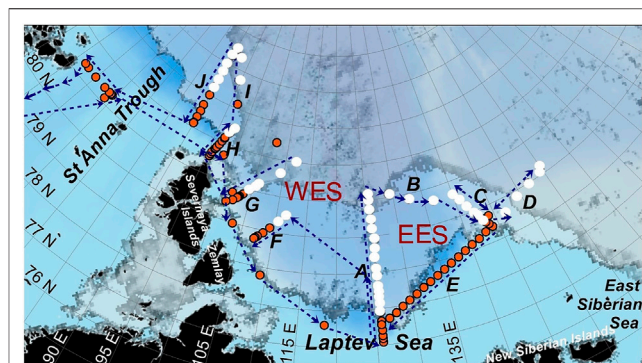


FIGURE 1 | Sea ice concentration [University of Bremen, (Spren et al., 2008)] on August 15th (light grey/translucent) and September 15th (dark grey/translucent) is shown together with sampling sites in open water (red) and ice-covered (white) regions. Blue arrows indicate the track of the R/V “Akademik Fedorov”.

melt and their mixing into the CHL. We show that the CH_4 plumes in the PML on the ECS are induced by the melt of mainly estuarine ice.

2 MATERIALS AND METHODS

We used CH_4 , total alkalinity and thermohaline observations collected at ten sections (Figure 1) over the Eurasian continental slope (ECS) of the Arctic Ocean from the St. Anna Trough to the East Siberian Sea during the Nansen and Amundsen Basins Observational System (NABOS, <https://uaf-iarc.org/NABOS/>) cruise onboard R/V “Akademik Fedorov” from August to September, 2013.

2.1 Satellite-Based Applications to Invest Sea Ice Conditions During Expedition

In order to determine the pathways and source regions of the ice along the sampling sections, we utilized the Lagrangian ice tracking tool, ICETrack. ICETrack makes use of low-resolution sea ice motion and concentration products and has been widely used in previous studies to identify age and origin of sea ice, as well as conditions along pathways (e.g. Belter et al., 2021; Krumpfen et al., 2021). A comparison of the satellite-based motion estimates of ICETrack with buoy data has shown that the deviation between real and virtual tracks is rather small (60 ± 24 km after 320 days, Krumpfen et al., 2020). For an in-depth method, data product and setup description, we refer to Krumpfen et al., 2019).

2.2 Thermohaline Observations, Sampling and Analysis

Profiles of salinity and temperature in the water column were obtained using a conductivity–temperature–depth (CTD) system. The principal device used, was a Sea-Bird SBE911. At selected CTD station a 24-Niskin bottle rosette was used to collect the

water samples for CH₄ and total alkalinity (TA) analysis every 10 m along the top 100 m. Under heavy ice condition sampling was carried out from fractures or leads.

Samples for CH₄ measurements were collected in 30, 100, 200 ml glass vials, taking care to avoid entrainment of bubbles while filling bottles, alkalinized up to pH 12, then sealed with rubber stoppers and aluminum caps. To avoid the risk of contamination samples were collected first followed by TA. CH₄ samples were stored in a refrigerator at 4° in the darkness until measuring in the land laboratory within 1 month after the cruise. CH₄ concentrations were measured by using a gas chromatograph with a flame ionization detector (Shimadzu, GA-8A) with an instrumental precision 1%. The analytical error for measurement was 3%.

The CH₄ saturations with respect to atmospheric equilibrium were calculated by applying the equilibrium concentration of CH₄ in sea water with the atmosphere as function of temperature and salinity (Wiesenburg and Guinasso, 1979). We used an atmospheric mole fraction of 1.91 ppm, i.e. the monthly mean from September, 2013 (Data provided by NOAA Global sampling networks, sampling Hydrometeorological Observatory of Tiksi, <http://www.esrl.noaa.gov>).

The fluxes (F, nMol/m² day) of CH₄ across the air-sea interface were calculated in accordance to Wanninkhof (1992), using the equation

$$F = K_w \times (C_w - C_a),$$

where K_w is the gas transfer velocity for CH₄, C_w is the measured CH₄ concentration in surface water, C_a is the equilibrium concentration of CH₄ at surface water temperature and salinity calculated using the measured CH₄ atmospheric mixing ratio and the Bunsen solubility coefficient taken from Wiesenburg and Guinasso, 1979. We have estimated K_w depending on wind speed (u) as described in Wanninkhof (1992):

$$K_w = 0.31 \times u^2 (Sc/660)^{-0.5}$$

Following Wanninkhof (1992), the appropriate Schmidt number (Sc) for CH₄ was calculated using the surface water temperature dependent polynomial relationship.

The relationship between TA and salinity was used to identify the freshwater fractions of sea ice melt or estuarine ice melt waters in the PML (Macdonald et al., 2002; Yamamoto-Kawai et al., 2005; Fransson et al., 2009; Alkire et al., 2019). For TA samples were collected into borosilicate glass flasks (125-ml) pre-treated with saturated mercuric chloride solution (200 μL); the bottles were sealed and stored until following analysis, which was carried out on board by an automated open-cell potentiometric titration (Haraldsson et al., 1997), with precision of ±1 μmol/L.

3 RESULTS

3.1 Weather and Ice Conditions During Sampling: On-Site Observations and Satellite-Based Assessments

Our first five stations near the ice edge covered a route ~80 miles apart the eastern Laptev Sea shelf break for the August 24–26th

period. Section A (**Figure 1**, along 126°E longitude) was carried out August 27–28th. No ice was present at the southern stations while mid and northern stations were sampled in an area with ice concentration >90 and 70–80%, respectively. Ice thickness ranged between 70 and 100 cm at the mid stations and 40–60 cm at the northern stations. The ice was first-year ice, substantially rotten and melted from below. For August 29–31st, three northern stations at section C were visited before the termination of sampling due to a consolidated heavy ice pack. Southern stations along the ice edge, were occupied on August 31st. On the next day, the stations along the ice edge towards section D were done. At ~153°E the thickness of the heavy consolidated pack ice reached 2 m. For September 4–6th section E was carried out. On September 8th, we started section F (crossing the Laptev Sea slope at 110°E). On September 10th, section F was interrupted at the middle of the slope by storm conditions. More specifically, the wind speed exceeded 18 m/s and the wave height exceeded 3 m. Work at section G (105°E) started in the marginal ice zone at the northern stations and was finalized at Severnaya Zemlya shelf on September 13th. The same day, we sampled section H at 95°E. Due to the presence of heavy pack ice, section I was started at 84°30'N and, interrupted by a storm, on September 16th. On September 17th we resumed sampling on section J along 90°E. However, a strong storm prevented sampling at the upper slope points. On September 18th and, 19th we sampled the final section across St. Anna Trough.

3.2 Water Mass Properties

A typical vertical structure of surface waters in the Eurasian sector of the Arctic Ocean consists of two layers—the Polar Mixed Layer (PML) and the Cold Halocline Layer (CHL) (Alkire et al., 2017).

The PML extends from the ocean surface to the ~20–55 m depths, and is characterized by vertical uniform distributions of temperature and salinity. Following Jones (2001), the base of the PML is associated with salinities ≤33 psu, but a wide range of temperatures. In line with that, in summer, 2013 the temperature of the PML varied between –1.78 and 2.51°C in the ice-free areas and between –0.137 and –1.781°C in the areas covered by sea ice.

Below the PML, strong vertical gradients of salinity accompanied by negligible gradients of temperature and a relatively weak T–S slope form the CHL. Strong salinity gradients in the CHL suggest the increased density stratification that suppresses diapycnal mixing between the upper and intermediate ocean layers (e.g., Rudels et al., 1996). In 2013, the CHL was localized between 20 and 80 m depths, slightly deepening in the eastern sector of the Makarov Basin. The CHL salinities varied between 33.0 and 34.0 psu (e.g., Alkire et al., 2017), whereas the temperature range was from –1.80°C to –0.1°C.

3.3 CH₄ Distributions

According to regional patterns, in our study, we divided the research area into two sectors: western and eastern ECS.

The western sector (further the western sector of the ECS, WES) comprises the sections located from the St Anna Trough up to the section A at 126°E (**Figure 1**, Sections A, F, G, H, I, J.). The eastern sector (further the eastern sector of the ECS, EES)

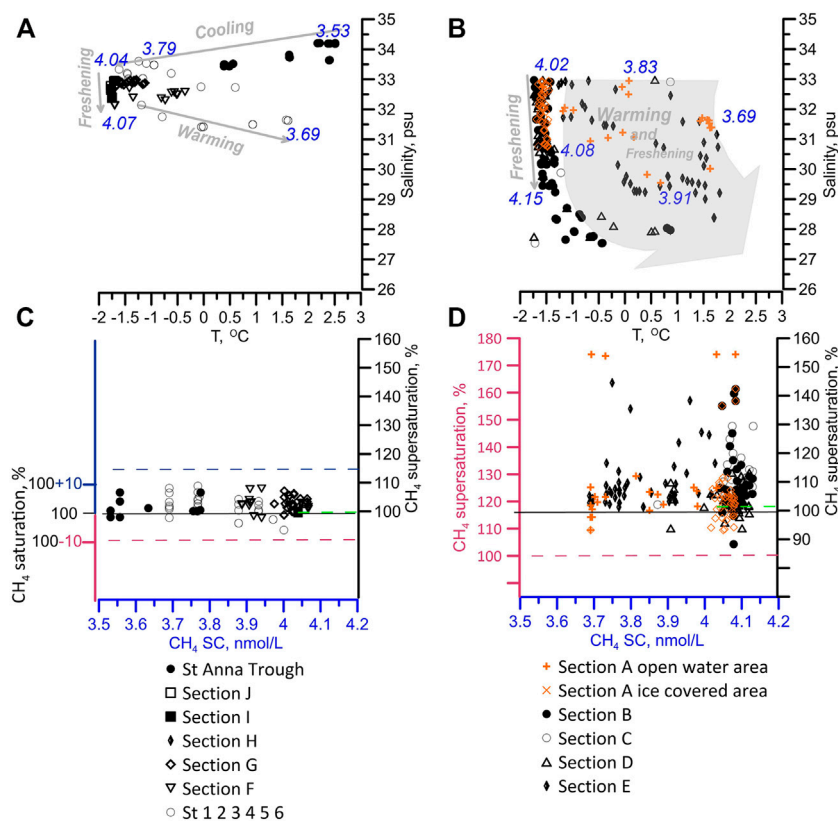


FIGURE 2 | The effect of the CH_4 solubility on the level of CH_4 saturation, related to the atmospheric equilibrium in the PML. The (A,B) gives the CH_4 solubility concentration (blue numbers) calculated in relation to the water temperature and salinity. The arrows show the dominant effect of either cooling or warming and freshening in the WES (A), and EES (B). The (C,D) shows the shift related to the saturation induced by changing solubility (dashed lines): in blue (cooling), in green (freshening), and in red (warming) in the WES (C) and EES (D). The shift in saturation forced by predominantly by warming (left red axes) consisted in real saturation (right black axes) (D). Orange symbols indicate the reference section A. In the WES the enhanced solubility masked the CH_4 supersaturation caused by marine sources. In the EES, CH_4 supersaturation is clearly induced by marine CH_4 sources.

comprises sections located to east from the Lomonosov Ridge (Figure 1, Sections B, C, D, E).

In the PML the highest CH_4 concentrations detected were 5.81 nmol/L, which reflected an average CH_4 super-saturation (154%) with respect to the atmospheric equilibrium. The mean CH_4 concentrations increased from 4.03 nmol/L (standard error, SE = 0.18) in the WES up to 4.25 nmol/L (mean, SE = 0.12) in the EES. This corresponded to a slightly increase of the CH_4 super-saturation from 105 to 107% in the WES and EES, respectively. Unlike the WES, where CH_4 saturation was the same for the ice-covered and ice-free areas, in the EES, CH_4 concentration at ice-free stations were 4.23 nmol/L (mean, SE = 0.19) that corresponded to a CH_4 super-saturation of 110.2%. At the ice-covered stations, the mean CH_4 concentration was 4.44 nmol/L (SE = 0.18), which corresponded to a CH_4 super-saturation of 109% at ice-covered stations.

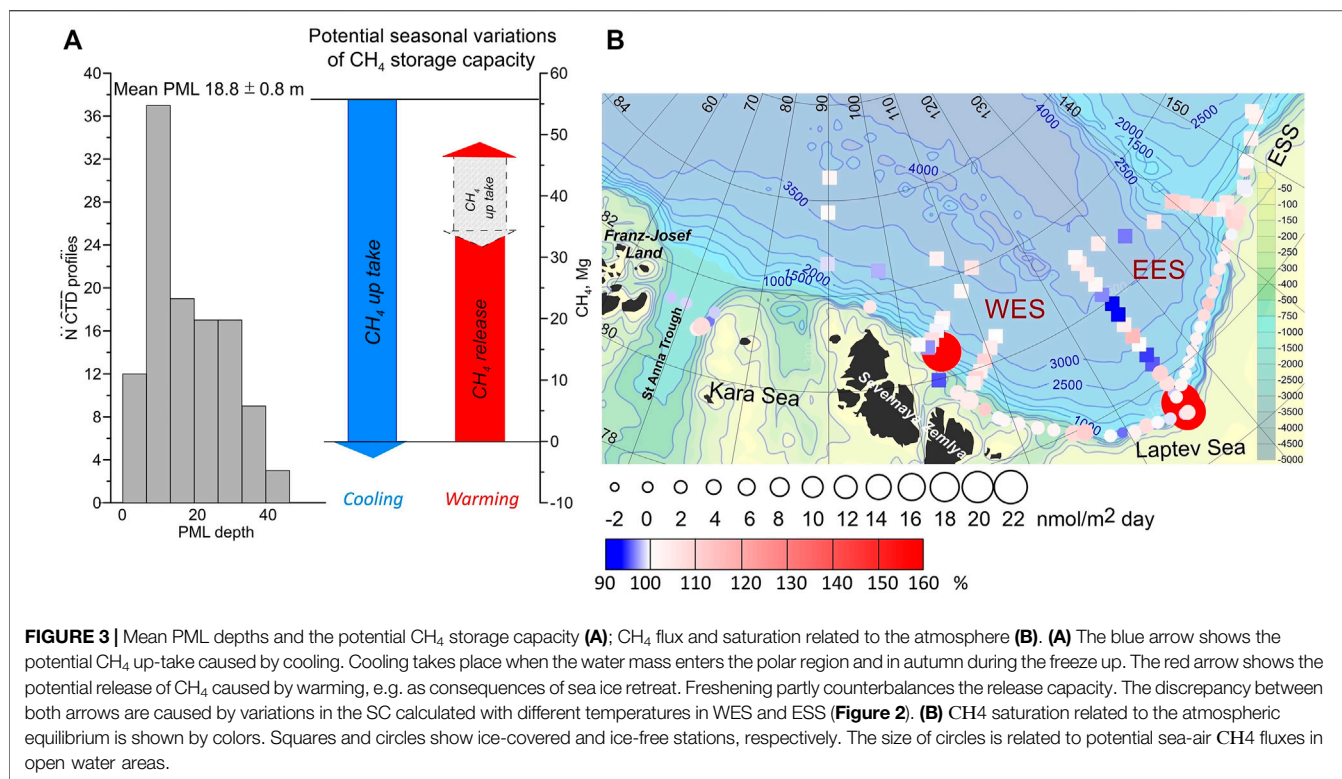
In the CHL the CH_4 concentrations increased from 3.49 nmol/L in the WES to 5.69 nmol/L in the ESL. Those corresponded to CH_4 saturation from 96.7 to 145%. In the WES, the mean CH_4 concentrations were 4.13 nmol/L (SE = 0.19) corresponding to a CH_4 super-saturation of 104%. In the EES mean CH_4

concentration was 4.35 nmol/L (SE = 0.19), which correspond to a CH_4 saturation of 108%.

4 DISCUSSION

When entering through the St Anna Trough, pronounced cooling and freshening by sea ice melt created the PML (Rudels et al., 1996). The direction of the PML circulation is supposed to correspond to the current of warm saline AW underneath, mainly following the coastline eastward (Carmack et al., 2016). The thickness of the PML enhanced from ~20 m at 90°E to ~50 m at 125°E.

In mid of August ~85% of the research area was covered by sea ice while, sea ice progressively reduced to less than ~10% in mid of September. During sampling roughly 15% of the stations on the WES (Figure 1) and, 46% of the stations on the EES were still ice covered. The salinity profiles of the PML clearly reflected the different stages of sea ice melt (Figure 1, Figure 4, Figure 6). As the ongoing melt also affects the CH_4 solubility capacity (SC), we discuss the sea ice effects on the CH_4 saturation with respect to the atmospheric equilibrium in detail.



4.1 CH₄ Solubility Capacity of the Polar Mixed Layer

The cooling of the warm inflowing surface water and coexisting freshening due to sea ice melt or meteoric water enhanced the SC from 3.53 to 4.07 nmol/L in the PML from west to east (Figures 2A, B).

In the ice-covered PML in the WES, the SC increased at ~13% mainly by cooling of the water down to near the freezing point (-1.718°C ; $S\ 32.963\ \text{psu}$), while the freshening effect remained negligible ($<0.1\%$, $\Delta S = 0.838\ \text{psu}$). That increase in SC resulted in a slightly CH₄ under-saturation related to the atmospheric equilibrium (Figure 2).

In the ice-covered PML in the EES, the water temperature was mostly near the freezing point, while the cooling effect on the SC was still sustained, reflected by the under-saturation at some stations. That pointed to a restricted air-sea exchange mainly hampered by the ice coverage.

By comparison, in the ice-free PML in the WES, a seasonal warming up to 1.608°C , resulted in ~10% less SC, finally reflected in under-saturation down to ~90% (Figure 2).

Freshening by sea ice melt increased the SC from 4.02 to 4.08 nmol/L at northern ice-covered stations (Figures 2A, C), resulted in negligible increase in the SC (~1%) compared to the effect of simultaneously occurring warming. Under consideration of the variabilities in saturation by changes in the SC, we observed CH₄ supersaturation up to 153% caused by additional CH₄ discharged from marine sources.

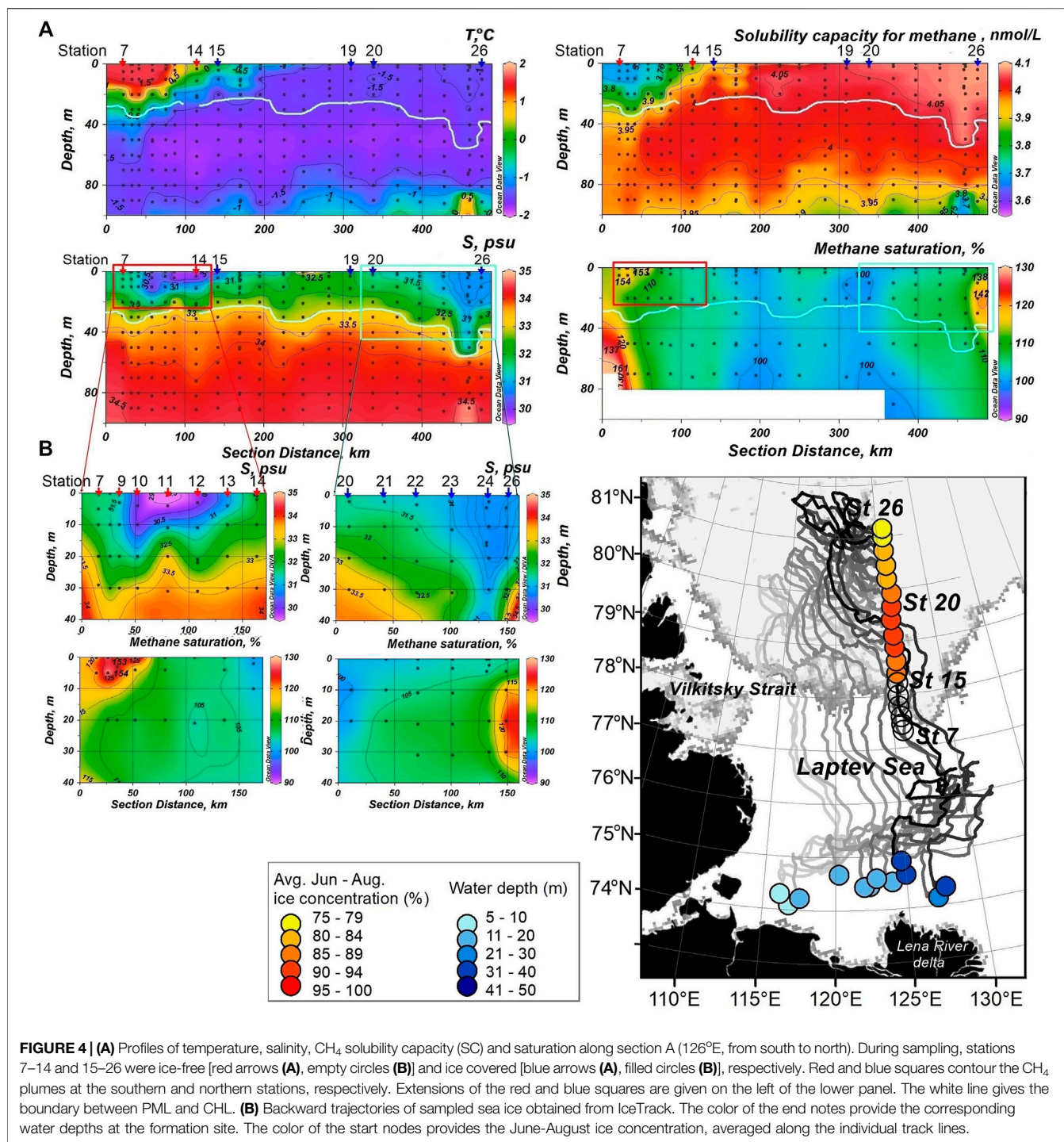
A combined effect of freshening and warming was observed in the EES including the reference section A, which served as a

boundary between the WES and EES (Figures 2B, D). The prevailing impact of warming to the decreased SC (11%) was attributed for all shelf break ice-free stations. By comparison, we observed the largest freshening, in the eastern EES, at the section C, increasing the SC to 4.15 nmol/L, which corresponded to a plus by ~2%.

The variation in the SC revealed the significance of surface warming and coherent freshening due to sea ice melt to the level of CH₄ saturation. Remarkably, the cooling of warm inflowing water in the WES results in an enhanced potential sink capacity for either atmospheric or marine CH₄ sources. However, this potential sink capacity seasonally shrinks by ice melt and subsequent warming of the melt water, while especially the degree of warming in summer, triggers the PML at the ECS switches to acting as a potential source for atmospheric CH₄ (Figure 3A).

4.2 The Potential CH₄ Storage Capacity of the Polar Mixed Layer

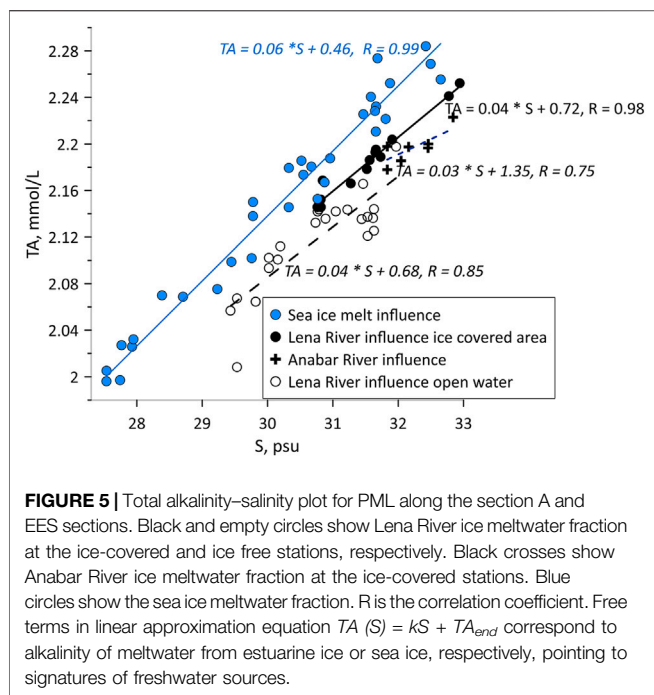
To assess the variation of potential sources and sink capacities in the upper PML by changing SC we estimated the CH₄ storage capacity within the upper 18.8 m. For the entire area covered by the 2013 NABOS II observations, we used the average PML depth of 18.8 m determined using high-resolution vertical profiles of the potential density (Figure 3A). We just considered the surface layer as a layer mainly favored to be influenced by sea-air gas exchange. Then we multiplied that value to the square of the research area and ΔSC in g/m^3 .



The locally restricted cooling of the inflowing warm surface water resulted in a potential CH₄ uptake of ~4.99 Mg (10⁶ g) CH₄. We considered this cooling effect exclusively for the region west of 90°E (section J), which corresponded to an area ~30,065 km².

In addition, cooling in autumn down to the freezing temperature occurs in the whole research area (335,778 km²). An assessment of the potential uptake capacity results in ~55.70 Mg of CH₄ (Figure 3A).

Under the assumption that the whole area becomes ice free in summer, the seasonal warming will result in 12% less SC tending to balance the relicts of the cooling effect (Figure 3A). Then up to ~46.58 Mg (10⁶ g) CH₄ might be potentially released from the ECS to the atmosphere. However, in summer 2013, ~66% of the research area was still ice covered, resulting in a two thirds smaller amount.



The seasonal changing storage capacity reveals the buffer capacity of the PML for atmospheric or marine-sourced CH_4 . While mostly annually balanced, the seasonal stored CH_4 might be reduced by ongoing oxidation in surface water. Studies considering CH_4 oxidation report low oxidation rates in surface waters of other Arctic regions (Mau et al., 2013; Mau et al., 2017; Damm et al., 2015; Uhlig and Loose 2017) but oxidation rate measurements are needed to verify if oxidation acts as CH_4 sink in the PML at the ECS.

Seasonal freshening enhanced the SC just by $\sim 3.2\%$, resulting in a potential uptake of ~ 13.17 Mg CH_4 . That contribution is small in comparison to the cooling/warming effect on the SC. However, summer sea ice retreat increases the seasonal ice melt at the ECS (Krumpfen et al., 2019). That reinforces the freshening effect. In addition, enhanced discharge of Siberian River water (McClelland et al., 2006; Overeem and Syvitski, 2016), which contributes approximately 40% of total freshwater into the Arctic Ocean (Serreze et al., 2006; Haine et al., 2015), will also contribute to increase the CH_4 uptake capacity in the coming decades.

4.3 CH_4 Excess in the Polar Mixed Layer

In summer, the surface water in the central Laptev Sea is reported to be slightly CH_4 supersaturated with spatial restricted hotspots of enhanced CH_4 excess (Thornton et al., 2016). In accordance, we detected CH_4 super-saturation up to $\sim 142\%$ in still ice covered and up to $\sim 154\%$ in ice-free PML. Further, we also revealed a pronounced spatial heterogeneity in the CH_4 excess (Figure 4A). Both aspects clearly point to a locally induced CH_4 excess. Hence, we suggest sea ice as the source for CH_4 excess, and the ongoing

melt of single ice floes as the process, which causes the heterogeneity in the excess (Damm et al., 2015; Damm et al., 2018; Verdugo et al., 2021). Certain features of local CH_4 release from sea ice into the PML during melt are shown at the section A and discussed in more detail below.

At the southern ice-free stations a CH_4 plume was directly located near the surface of the PML. Remarkably, the plume showed gradients in CH_4 concentration and also in salinity. Both, CH_4 concentration and salinity decreased from south to north (Sts 7–14). That pattern pointed to the formation of the CH_4 plume during the early stage of melt, i.e. when brine charged with CH_4 had been released from sea ice. By comparison, at the northern stations (Sts 12–14) the plume had been subsequently diluted on top during ongoing melt when brine release ceased and remain freshwater discharged. While at the southern stations the ice had being drifted away just before dilution by freshwater started, leaving the plume on top of the PML undiluted (Figure 4A).

At the northern ice-covered stations (Sts 25, 26), a CH_4 plume was disposed at the depth range 10–30 m (Figure 4A). Notably, the plume position pointed to CH_4 transport dissolved in brine downward during early stages of sea ice melt (Verdugo et al., 2021). Also the lower sea ice concentration at the northern compared to the southern stations (Figure 4B), pointed to different stages of ice melt.

This counterintuitive pattern is corroborated by the salinity gradients. Further, tracing the drift pattern, it is obvious that ice at the southern and northern part of the section was formed on the inner Laptev Sea shelf impacted by the Anabar and the Lena River waters, respectively (Figure 4B). The ice formed in the Anabar Estuary was less saline because the native winter salinity is < 10 psu (Dmitrenko et al., 2005) than formed in the Lena Estuary, where native winter salinity is 22–28 psu (Dmitrenko et al., 2005). The low salinity of the ice formed in the Anabar estuary caused the relatively slower ice melt at the stations in the middle of the section.

The CH_4 plumes were directly related to initial CH_4 concentration in the ice. CH_4 uptake into sea ice occurs during ice formation from supersaturated seawater (Crabeck et al., 2014; Zhou et al., 2014; Damm et al., 2018). The shallow Laptev Sea shelf is a significant sources of CH_4 (Shakhova et al., 2015; Baranov et al., 2020) and CH_4 supersaturation in shelf water in summer is reported (Bussmann et al., 2017; Sapart et al., 2017; Savvichev et al., 2018).

The river estuaries are characterized by high sedimentation rates (Bauch et al., 2001; Stein et al., 2001; Han, 2014), which exert the dominant control on benthic escape of CH_4 at the sediment-water interface in the shallow Laptev Sea (Puglioni et al., 2020). Further, CH_4 uptake during sea ice formation is favored on shallow shelves as cooling during freeze creates convection down to the bottom. This convective mixing enhances the turbulence, initiates resuspension of sediments, and eventually CH_4 release from bottom (Wegner et al., 2017; Damm et al., 2021). Convection also enables rapid transport of CH_4 to the sea surface and hence the uptake into sea ice during freeze events (Damm et al., 2007; Damm et al., 2021).

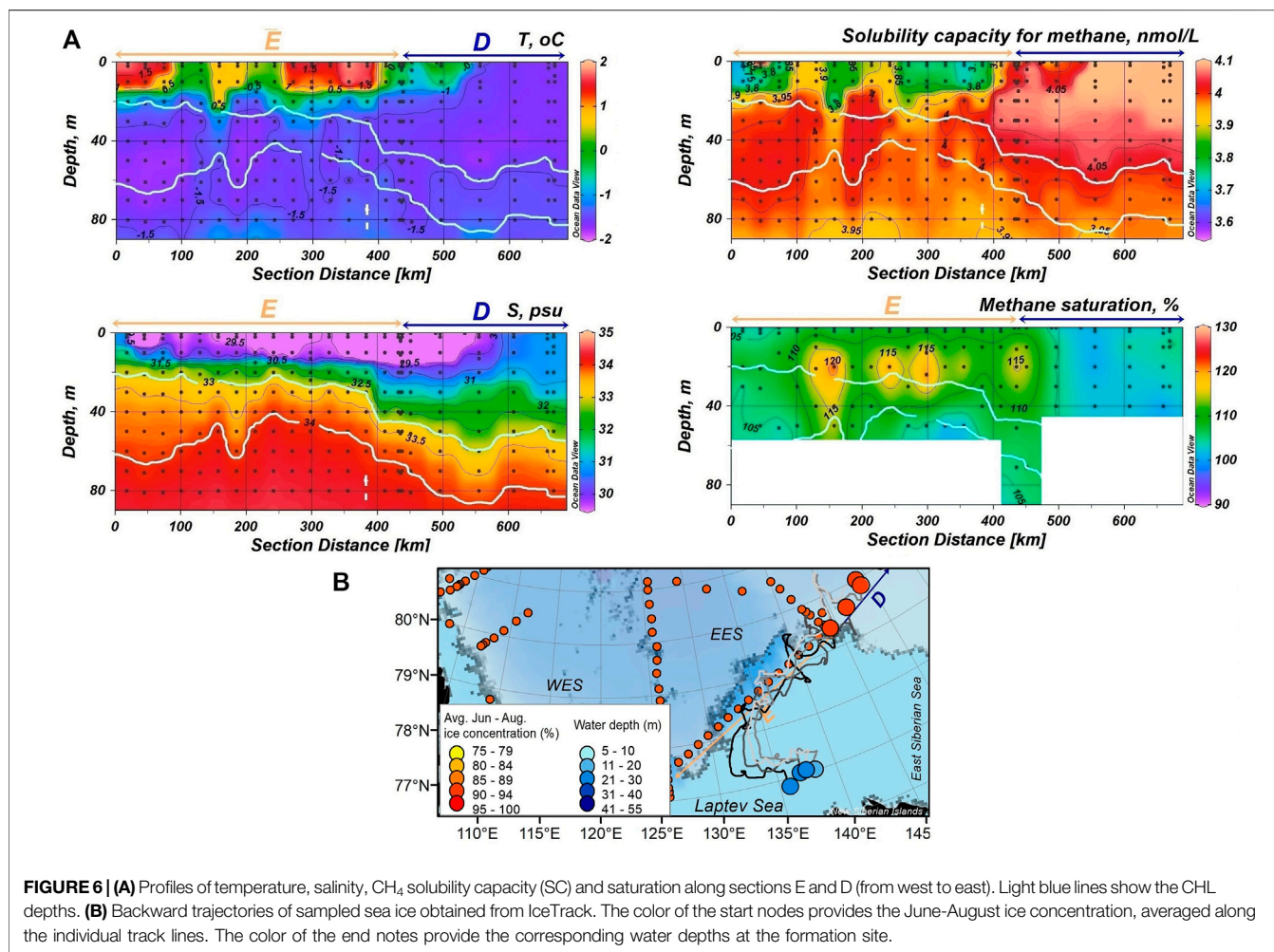


FIGURE 6 | (A) Profiles of temperature, salinity, CH₄ solubility capacity (SC) and saturation along sections E and D (from west to east). Light blue lines show the CHL depths. **(B)** Backward trajectories of sampled sea ice obtained from IceTrack. The color of the start nodes provides the June-August ice concentration, averaged along the individual track lines. The color of the end nodes provide the corresponding water depths at the formation site.

The satellite-based backtracking approach of the ice has shown that ice positioned at the northern plume stations was formed in the Anabar-Lena polynya with a water-depth between 30–50 m before it was advected north by prevailing offshore winds (Krumpfen et al., 2016, Krumpfen et al., 2019) (Figure 4B).

In addition, the TA/S ratio at those plume stations (0.72, Figure 5) was close to the TA of the Lena River water (0.78 mmol/L from Cooper et al., 2008) clearly pointing to freshening by Lena River ice meltwater fraction. The contribution of ice formed in the estuaries of the large Siberian Rivers to the ice cover in Nansen Basin was reported early (Eicken et al., 2005). Hence, we suggest the existence of ice predominantly formed in the external Lena River estuary on the Laptev Sea shelf and therefore argue for CH₄ uptake from sediments into Lena estuary ice during its formation in autumn. Also at the southern ice-free stations the PML contained Lena River ice meltwater fraction shown by TA/S signal (0.68, Figure 5).

In comparison to both plume regions, we detected less CH₄ supersaturation (up to 109%) at ice-covered stations in the middle of the section (Sts 15–19, Figure 4A). Backward drift

trajectories pointed to the southwestern Laptev Sea shelf with depths ranged from 5 to 30 m, influenced by the Anabar River runoff, as the region for ice formation. The TA/S ratio (Figure 5) corroborated the Anabar River waters (Zhulidov and Emetz, 1991) as source water, and the western area of the Laptev Sea as the region for ice formation. The low salinity of the Anabar estuarine-ice caused less CH₄ amount, captured during freezing and the relatively slower ice melt at the stations in the middle of the section.

4.4 The Subsequent Fate of the PML—CH₄ Excess

4.4.1 Potential CH₄ flux to the Atmosphere

As long as a supersaturation of CH₄ in the PML exists, CH₄ might also escape to the atmosphere. Sea-air flux is mainly favored at the end of the ice-free season when cooling and storm events diminish the water stratification. Since the atmosphere potentially acts as final sink for the marine CH₄ that is seasonally stored in sea ice we have calculated the sea-air CH₄ flux.

The PML on the ECS was weakly supersaturated with CH₄, and hence a potential slight net source for the atmosphere during the summer (**Figure 3B**). In total, the CH₄ concentration exceeded the atmospheric equilibrium at 0.22 nmol/L. The average sea-air CH₄ flux, calculated for open water, was 2.0 nmol/m²day. A slightly higher flux was calculated for the outer shelf of the EES and on the external Laptev Sea shelf at the southern stations along sections A and G (**Figure 3B**). Summarized, the low sea-air flux indicates the ECS as a potential source for atmospheric CH₄ mainly by strong wind loadings, i.e. during storm events.

4.4.2 Dilution of CH₄ Excess in the Polar Mixed Layer and Downward Mixing Into the Cold Halocline Layer

Rapid ice retreat and accompanying strong sea ice melt provided the largest contribution of fresh water to the upper part of the PML in 2013 (Itkin and Krumpfen, 2017). Hence, the level of CH₄ excess in the PML was mainly triggered by the dilution with freshwater during later stages of melt. This dilution effect and the potential mixing into deeper water masses are the main processes contributing to keep the estuarine and shelf-sourced CH₄ in the ocean. Apart from oxidation, dilution up to marine CH₄ background values in sea water finally encourage that the ocean acts as sink for marine CH₄ excess in Polar regions (Damm et al., 2021).

We detected CH₄ plumes crossing the boundary between PML and CHL at the ice-free eastern Laptev Sea shelf break (**Figure 6A**). That feature revealed the intrusion of water from the PML, including the CH₄ plume, into the CHL. The increased temperature within those intrusions, related the CHL at surrounding stations, corroborated the PML as the source of the CH₄ plumes (**Figure 6A**). Vertical mixing induced by eddies at the ice edge (Zhao et al., 2014; Pnyushkov et al., 2018) favored the intrusion of water from the PML into the upper CHL and thus the transport of shelf-sourced CH₄ into deeper water masses.

We discussed the plume formation as a result of CH₄ release from sea ice coupled to gravity brine drainage during the first melt stage (see above). Ongoing sea ice melt diluted the plume on top by freshwater discharge. Though, under the warm surface layer, the CH₄ plumes are sustained by the strong density gradient on the top while the vertical mixing between PML and CHL enabled a downward deepening of the CH₄ plumes (**Figure 6A**). The ice edge provides favorable conditions for eddy generation as specifically, convection by water cooling in leads generates a vertical dipole structure with a cyclonic eddy in the upper layer and an anticyclonic eddy in the CHL (Manley and Hunkins, 1985; Gupta et al., 2020; Meneghello et al., 2021). Further studies are needed to verify the role of eddies especially their enhanced lateral and vertical mixing capacity between certain water masses at the EES (Zhao et al., 2014; Pnyushkov et al., 2018) to contribute to the deepening of CH₄ plumes into subsurface waters.

Remarkably, we did not observe CH₄ plumes further east at the ice-covered shelf-break (Section D, **Figure 6A**). At these locations, sea ice melt had just began and CH₄ release from sea

ice, was still masked by the enhanced SC of the cold PML water. Further, ice drift trajectories indicated the area of sea ice formation in the shallow Laptev Sea shelf north from the New Siberian Islands (**Figure 6B**). In this area CH₄ supersaturation in seawater as a result of CH₄ release from the sediments under conditions of active turbulence are expected to be low (Puglini et al., 2020). Hence, the just slightly CH₄ super-saturation (up to 108%) corroborate the capturing of low amounts of CH₄ in sea ice on the shelf north from the New Siberian Islands.

CONCLUSION

We found a heterogeneous excess of CH₄ next to the surface in the PML and suggest that sea ice impacts on the amount and pathways of CH₄ on the ECS. On the one side, the cycle of sea ice formation and melt alters the solubility capacity of CH₄ in the surface waters, which ultimately affects its ability to act as a source or sink of atmospheric CH₄. On the other side, sea ice transports shelf-derived CH₄ to the open ocean, which likely acts as a CH₄ sink. It is noteworthy, that the largest CH₄ excess in the PML on the ECS is generated by melt of ice originated in outer river estuaries on the shallow Laptev Sea shelf.

The increased solubility capacity during cooling has shown that the PML on the ECS acts as a potential seasonal sink for atmospheric or marine CH₄. summer ice melt causes surface freshening and subsequent warming. The warming offsets the cooling effect and triggers the switching of the PML to act as a potential source of atmospheric CH₄ in summer. The joint effect of both processes creates the seasonal buffer capacity of the PML. summer sea ice retreat will increase the freshening effect, the buffer capacity and reinforce the sink function of the PML for CH₄.

Finally, Arctic amplification favors perennial sea ice retreat, and hence, we expect that larger amounts of freshwater will dilute the CH₄ excess in surface water which eventually restricts CH₄ flux into the atmosphere.

These linkages should be considered when assessing CH₄ sources and sinks in the changing Arctic.

DATA AVAILABILITY STATEMENT

The datasets presented in this study can be found in online repositories. The names of the repository/repositories and accession number(s) can be found below: <https://uaf-iarc.org/nabos/>.

AUTHOR CONTRIBUTIONS

EV designed the study. EV and ED wrote the paper. EV sampled and analyzed the CH₄ data. AP sampled and analyzed the physical oceanography data and wrote the oceanography chapter. TK carried out sea ice trajectories and wrote the ice

trajectory part. All authors contributed to the interpretation of the data, the manuscript and the figures.

FUNDING

This study was performed in the framework of the state assignment of IO RAS (theme 0128-2021-0005); NSF funded IARC Program “Nansen and Amundsen Basins Observational System” (NABOS II; grant #1203473).

REFERENCES

- Alkire, M. B., Jacobson, A., Macdonald, R. W., and Lehn, G. (2019). Assessing the Contributions of Atmospheric/Meteoritic Water and Sea Ice Meltwater and Their Influences on Geochemical Properties in Estuaries of the Canadian Arctic Archipelago. *Estuaries and Coasts* 42, 1226–1248. doi:10.1007/s12237-019-00562-w
- Alkire, M. B., Polyakov, I., Rember, R., Pnyushkov, A., Ivanov, V., and Ashik, I. (2017). Combining Physical and Geochemical Methods to Investigate Lower Halocline Water Formation and Modification along the Siberian continental Slope. *Ocean Sci.* 13, 983–995. doi:10.5194/os-13-983-2017
- AMAP (2015). *Assessment 2015: Human Health in the Arctic*. Oslo, Norway: AMAP. Availableat: <https://www.amap.no>.
- Baranov, B., Galkin, S., Vedenin, A., Dozorova, K., Gebruk, A., and Flint, M. (2020). Methane Seeps on the Outer Shelf of the Laptev Sea: Characteristic Features, Structural Control, and Benthic Fauna. *Geo-mar Lett.* 40, 541–557. doi:10.1007/s00367-020-00655-7
- Bauch, H. A., Mueller-Lupp, T., Taldenkova, E., Spielhagen, R. F., Kassens, H., Grootes, P. M., et al. (2001). Chronology of the Holocene Transgression at the North Siberian Margin. *Glob. Planet. Change* 31, 125–139. doi:10.1016/S0921-8181(01)00116-3
- Belter, H. J., Krumpfen, T., von Albedyll, L., Alekseeva, T. A., Birnbaum, G., Frolov, S. V., et al. (2021). Interannual Variability in Transpolar Drift Summer Sea Ice Thickness and Potential Impact of Atlantification. *The Cryosphere* 15, 2575–2591. doi:10.5194/tc-15-2575-2021
- Berchet, A., Bousquet, P., Pison, I., Locatelli, R., Chevallier, F., Paris, J.-D., et al. (2016). Atmospheric Constraints on the Methane Emissions from the East Siberian Shelf. *Atmos. Chem. Phys.* 16, 4147–4157. doi:10.5194/acp-16-4147-2016
- Bussmann, I., Hackbusch, S., Schaal, P., and Wichels, A. (2017). Methane Distribution and Oxidation Around the Lena Delta in Summer 2013. *Biogeosciences* 14, 4985–5002. doi:10.5194/bg-14-4985-2017
- Carmack, E. C., Yamamoto-Kawai, M., Haine, T. W. N., BaconBluhm, S., Bluhm, B. A., Lique, C., et al. (2016). Freshwater and its Role in the Arctic Marine System: Sources, Disposition, Storage, export, and Physical and Biogeochemical Consequences in the Arctic and Global Oceans. *J. Geophys. Res. Biogeosci.* 121, 675–717. doi:10.1002/2015JG003140
- Chuvilin, E., Ekimova, V., Davletshina, D., Sokolova, N., and Bukhanov, B. (2020). Evidence of Gas Emissions from Permafrost in the Russian Arctic. *Geosciences* 10, 383. doi:10.3390/geosciences10100383
- Cooper, L. W., McClelland, J. W., Holmes, R. M., Raymond, P. A., Gibson, J. J., Guay, C. K., et al. (2008). Flow-weighted Values of Runoff Tracers ($\delta^{18}O$, DOC, Ba, Alkalinity) from the Six Largest Arctic Rivers. *Geophys. Res. Lett.* 35, L18606. doi:10.1029/2008GL035007
- Crabeck, O., Delille, B., Thomas, D. N., Geilfus, N. X., Rysgaard, S., and Tison, J. L. (2014). CO₂ and CH₄ in Sea Ice from a Subarctic Fjord. *Biogeosciences Discuss.* 11, 4047–4083. doi:10.5194/bgd-11-4047-2014
- Damm, E., Bauch, D., Krumpfen, T., Rabe, B., Korhonen, M., Vinogradova, E., et al. (2018). The Transpolar Drift Conveys Methane from the Siberian Shelf to the central Arctic Ocean. *Sci. Rep.* 8, 4515. doi:10.1038/s41598-018-22801-z
- Damm, E., Ericson, Y., and Falck, E. (2021). Waterside Convection and Stratification Control Methane Spreading in Supersaturated Arctic Fjords (Spitsbergen). *Continental Shelf Res.* 224, 104473. doi:10.1016/j.csr.2021.104473

ACKNOWLEDGMENTS

We thanked the captain and crew of R/V Akademik Fedorov for their support during the NABOS 2013 cruise. We are grateful to I. Repina for providing wind data. We also thank M. Angelopoulos for his comments on an earlier version of this paper. VI acknowledges support by the Interdisciplinary Scientific and Educational School of M.V. Lomonosov Moscow State University Future Planet and Global Environmental Change, AP acknowledges support by the NSF (grant #1724523).

- Damm, E., Rudels, B., Schauer, U., Mau, S., and Dieckmann, G. (2015). Methane Excess in Arctic Surface Water- Triggered by Sea Ice Formation and Melting. *Sci. Rep.* 5, 16179. doi:10.1038/srep16179
- Damm, E., Schauer, U., Rudels, B., and Haas, C. (2007). Excess of Bottom-Released Methane in an Arctic Shelf Sea Polynya in winter. *Continental Shelf Res.* 27, 1692–1701. doi:10.1016/j.csr.2007.02.003
- Dmitrenko, I. A., Kirillov, S. A., Tremblay, L. B., Bauch, D., and Willmes, S. (2009). Sea-ice Production over the Laptev Sea Shelf Inferred from Historical Summer-To-winter Hydrographic Observations of 1960s–1990s. *Geophys. Res. Lett.* 36, L13605. doi:10.1029/2009GL038775
- Dmitrenko, I., Tyshko, K., Kirillov, S., Eicken, H., HolemannKassense, J. H., and Kassens, H. (2005). Impact of Flaw Polynyas on the Hydrography of the Laptev Sea. *Glob. Planet. Change* 48, 9–27. doi:10.1016/j.gloplacha.2004.12.016
- Eicken, H., Dmitrenko, I., Tyshko, K., Darovskikh, A., Dierking, W., Blahak, U., et al. (2005). Zonation of the Laptev Sea Landfast Ice Cover and its Importance in a Frozen Estuary. *Glob. Planet. Change* 48, 55–83. doi:10.1016/j.gloplacha.2004.12.005
- Fransson, A., Chierici, M., and Nojiri, Y. (2009). New Insights into the Spatial Variability of the Surface Water Carbon Dioxide in Varying Sea Ice Conditions in the Arctic Ocean. *Continental Shelf Res.* 29, 1317–1328. doi:10.1016/j.csr.2009.03.008
- Genz, T., Damm, E., Schneider von DeimlingDeimling, J., Mau, S., McGinnis, D. F., and Schlüter, M. (2014). A Water Column Study of Methane Around Gas Flares Located at the West Spitsbergen continental Margin. *Continental Shelf Res.* 72, 107–118. doi:10.1016/j.csr.2013.07.013
- Günther, F., Overduin, P. P., Yakshina, I. A., Opel, T., Baranskaya, A. V., and Grigoriev, M. N. (2015). Observing Muostakh Disappear: Permafrost Thaw Subsidence and Erosion of a Ground-Ice-Rich Island in Response to Arctic Summer Warming and Sea Ice Reduction. *The Cryosphere* 9, 151–178. doi:10.5194/tc-9-151-2015
- Gupta, M., Marshall, J., Song, H., Campin, J. M., and Meneghello, G. (2020). Sea-Ice Melt Driven by Ice-Ocean Stresses on the Mesoscale. *J. Geophys. Res. Oceans* 125, e2020JC016404. doi:10.1029/2020JC016404
- Haine, T. W. N., Curry, B., Gerdes, R., Hansen, E., Karcher, M., Lee, C., et al. (2015). Arctic Freshwater export: Status, Mechanisms, and Prospects. *Glob. Planet. Change* 125, 13–35. doi:10.1016/j.gloplacha.2014.11.013
- Haraldsson, C., Anderson, L. G., Hassellöv, M., Hulth, S., and Olsson, K. (19971997). Rapid, High-Precision Potentiometric Titration of Alkalinity in Ocean and Sediment Pore Waters. *Deep Sea Res. Part Oceanographic Res. Pap.* 44, 2031–2044. doi:10.1016/S0967-0637(97)00088-5
- IPCC (2019). *Special Report on the Ocean and Cryosphere in a Changing Climate*. Editors H.-O. Pörtner, D. C. Roberts, V. Masson-Delmotte, P. Zhai, and M. Tignor. Chapter III. Geneva. Availableat: <https://www.ipcc.ch/srocc/chapter/chapter-3-2/>.
- Itkin, P., and Krumpfen, T. (2017). Winter sea ice export from the Laptev Sea preconditions the local summer sea ice cover. *The Cryosphere Discussions*, 1–15. doi:10.5194/tc-2017-28
- Iwamoto, K., Ohshima, K. I., and Tamura, T. (2014). Improved Mapping of Sea Ice Production in the Arctic Ocean Using AMSR-E Thin Ice Thickness Algorithm. *J. Geophys. Res. Oceans* 119, 3574–3594. doi:10.1002/2013jc009749
- Jones, E. P. (2001). Circulation in the Arctic Ocean. *Polar Res.* 20 (2), 139–146. doi:10.3402/polar.v20i2.6510
- Krumpfen, T., Belter, H. J., Boetius, A., Damm, E., Haas, C., Hendricks, S., et al. (2019). Arctic Warming Interrupts the Transpolar Drift and Affects Long-

- Range Transport of Sea Ice and Ice-Rafted Matter. *Sci. Rep.* 9, 5459. doi:10.1038/s41598-019-41456-y
- Kruppen, T., Birrien, F., Kauker, F., Rackow, T., von Albedyll, L., Angelopoulos, M., et al. (2020). The MOSAiC Ice Floe: Sediment-Laden Survivor from the Siberian Shelf. *The Cryosphere* 14, 2173–2187. doi:10.5194/tc-14-2173-2020
- Kruppen, T., Gerdes, R., Haas, C., Hendricks, S., Herber, A., Selyuzhenok, V., et al. (2016). Recent Summer Sea Ice Thickness Surveys in Fram Strait and Associated Ice Volume Fluxes. *The Cryosphere* 10, 523–534. doi:10.5194/tc-10-523-2016
- Kruppen, T., von Albedyll, L., Goessling, H. F., Hendricks, S., Juhls, B., Spreen, G., et al. (2021). MOSAiC Drift Expedition from October 2019 to July 2020: Sea Ice Conditions from Space and Comparison with Previous Years. *The Cryosphere* 15, 3897–3920. doi:10.5194/tc-15-3897-2021
- Kruppen, T., Willmes, S., Morales Maqueda, M. A., Haas, C., Hölemann, J. A., Gerdes, R., et al. (2011). Evaluation of a Polynya Flux Model by Means of thermal Infrared Satellite Estimates. *Ann. Glaciol.* 52 (57), 52–60. doi:10.3189/172756411795931615
- Macdonald, R. W., McLaughlin, F. A., and Carmack, E. C. (2002). Fresh Water and its Sources during the SHEBA Drift in the Canada Basin of the Arctic Ocean. *Deep Sea Res. Part Oceanographic Res. Pap.* 49, 1769–1785. doi:10.1016/S0967-0637(02)00097-3
- Manley, T. O., and Hunkins, K. (1985). Mesoscale Eddies of the Arctic Ocean. *J. Geophys. Res.* 90 (C3), 4911–4930. doi:10.1029/jc090ic03p04911
- Markus, T., Stroeve, J. C., and Miller, J. (2009). Recent Changes in Arctic Sea Ice Melt Onset, Freezeup, and Melt Season Length. *J. Geophys. Res.* 114, C12024. doi:10.1029/2009JC005436
- Mau, S., Blees, J., Helmke, E., Niemann, H., and Damm, E. (2013). Vertical Distribution of Methane Oxidation and Methanotrophic Response to Elevated Methane Concentrations in Stratified Waters of the Arctic Fjord Storfjorden (Svalbard, Norway). *Biogeosciences* 10, 6267–6278. doi:10.5194/bg-10-6461-2013
- Mau, S., Römer, M., Torres, M. E., Bussmann, I., Pape, T., Damm, E., et al. (2017). Widespread Methane Seepage along the continental Margin off Svalbard - from Bjørnøya to Kongsfjorden. *Sci. Rep.* 7, 42997. doi:10.1038/srep42997
- McClelland, J. W., Déry, S. J., Peterson, B. J., Holmes, R. M., and Wood, E. F. (2006). A Pan-Arctic Evaluation of Changes in River Discharge during the Latter Half of the 20th century. *Geophys. Res. Lett.* 33, L06715. doi:10.1029/2006GL025753
- Meneghello, G., Marshall, J., Lique, C., Isachsen, P. E., Doddridge, E., Campin, J.-M., et al. (2021). Genesis and Decay of Mesoscale Baroclinic Eddies in the Seasonally Ice-Covered interior Arctic Ocean. *J. Phys. Oceanogr.* 51, 115–129. doi:10.1175/JPO-D-20-0054.1
- Myhre, C. L., Ferré, B., Platt, S. M., Silyakova, A., Hermansen, O., Allen, G., et al. (2016). Extensive Release of Methane from Arctic Seabed West of Svalbard during Summer 2014 Does Not Influence the Atmosphere. *Geophys. Res. Lett.* 43 (9), 4624–4631. doi:10.1002/2016GL068999
- Overeem, I., and Syvitski, J. P. M. (2016). Shifting Discharge Peaks in Arctic Rivers, 1977–2007. *Geografiska Annaler. Ser. A, Phys. Geogr.* 92, 285–296. doi:10.1111/j.1468-0459.2010.00395.x
- Pnyushkov, A., Polyakov, I. V., Padman, L., and Nguyen, A. T. (201820182). Structure and Dynamics of Mesoscale Eddies over the Laptev Sea continental Slope in the Arctic Ocean. *Ocean Sci.* 14, 1329–1347. doi:10.5194/os-14-1329-2018
- Puglini, M., BrovkinRegnier, V. P., Regnier, P., and Arndt, S. (2020). Assessing the Potential for Non-turbulent Methane Escape from the East Siberian Arctic Shelf. *Biogeosciences* 17, 3247–3275. doi:10.5194/bg-17-3247-2020
- Reagan, M. T., and Moridis, G. J. (2008). Dynamic Response of Oceanic Hydrate Deposits to Ocean Temperature Change. *J. Geophys. Res.* 113, C12023. doi:10.1029/2008JC004938
- Rudels, B., Anderson, L. G., and Jones, E. P. (1996). Formation and Evolution of the Surface Mixed Layer and Halocline of the Arctic Ocean. *J. Geophys. Res.* 101 (C4), 8807–8821. doi:10.1029/96jc00143
- Rudels, B., Jones, E. P., Schauer, U., and Eriksson, P. (2004). Atlantic Sources of the Arctic Ocean Surface and Halocline Waters. *Polar Res.* 23 (2), 181–208. doi:10.3402/polar.v23i2.6278
- Sapart, C. J., Shakhova, N., Semiletov, I., Jansen, J., Szidat, S., Kosmach, D., et al. (2017). The Origin of Methane in the East Siberian Arctic Shelf Unraveled with Triple Isotope Analysis. *Biogeosciences* 14, 2283–2292. doi:10.5194/bg-14-2283-2017
- Savvichev, A. S., Kadnikov, V. V., Kravchishina, M. D., Galkin, S. V., Novigatskii, A. N., Sigalevich, P. A., et al. (2018). Methane as an Organic Matter Source and the Trophic Basis of a Laptev Sea Cold Seep Microbial Community. *Geomicrobiology J.* 35, 411–423. doi:10.1080/01490451.2017.1382612
- Screen, J. A., and Simmonds, I. (2010). The central Role of Diminishing Sea Ice in Recent Arctic Temperature Amplification. *Nature* 464 (7293), 1334–1337. doi:10.1038/nature09051
- Serreze, M. C., Barrett, A. P., Slater, A. G., Woodgate, R. A., Aagaard, K., Lammers, R. B., et al. (2006). The Large-Scale Freshwater Cycle of the Arctic. *J. Geophys. Res.* 111, C11010. doi:10.1029/2005JC003424
- Shakhova, N., Semiletov, I., and Chuvin, E. (2019). Understanding the Permafrost-Hydrate System and Associated Methane Releases in the East Siberian Arctic Shelf. *Geosciences* 9, 251. doi:10.3390/geosciences9060251
- Shakhova, N., Semiletov, I., Leifer, I., Sergienko, V., Salyuk, A., Kosmach, D., et al. (2014). Ebullition and Storm-Induced Methane Release from the East Siberian Arctic Shelf. *Nat. Geosci.* 7, 64–70. doi:10.1038/ngeo2007
- Shakhova, N., Semiletov, I., Salyuk, A., Yusupov, V., Kosmach, D., and Gustafsson, Ö. (2010). Extensive Methane Venting to the Atmosphere from Sediments of the East Siberian Arctic Shelf. *Science* 327, 1246–1250. doi:10.1126/science.1182221
- Shakhova, N., Semiletov, I., Sergienko, V., Lobkovsky, L., Yusupov, V., Salyuk, A., et al. (2015). The East Siberian Arctic Shelf: towards Further Assessment of Permafrost-Related Methane Fluxes and Role of Sea Ice. *Phil. Trans. R. Soc. A.* 373 (2052), 20140451. doi:10.1098/rsta.2014.0451
- Silyakova, A., Jansson, P., Serov, P., Ferré, B., Pavlov, A. K., Hattermann, T., et al. (2020). Physical Controls of Dynamics of Methane Venting from a Shallow Seep Area West of Svalbard. *Continental Shelf Res.* 194, 104030. doi:10.1016/j.csr.2019.104030
- Spreen, G., Kaleschke, L., and Heygster, G. (2008). Sea Ice Remote Sensing Using AMSR-E 89-GHz Channels. *J. Geophys. Res.* 113, C02S03. doi:10.1029/2005JC003384
- Stein, R., Boucsein, B., Fahl, K., Garcia de Oteyza, T., Knies, J., and Niessen, F. (2001). Accumulation of Particulate Organic Carbon at the Eurasian continental Margin during Late Quaternary Times: Controlling Mechanisms and Paleoenvironmental Significance. *Glob. Planet. Change* 31, 87–104. doi:10.1016/S0921-8181(01)00114-x
- Thornton, B. F., Geibel, M. C., Crill, P. M., Humborg, C., and Mörtz, C.-M. (2016). Methane Fluxes from the Sea to the Atmosphere across the Siberian Shelf Seas. *Geophys. Res. Lett.* 43, 5869–5877. doi:10.1002/2016GL068977
- Uhlig, C., and Loose, B. (2017). Using Stable Isotopes and Gas Concentrations for Independent Constraints on Microbial Methane Oxidation at Arctic Ocean Temperatures. *Limnol. Oceanogr. Methods* 15, 737–751. doi:10.1002/lom3.10199
- Verdugo, J., Damm, E., and Nikolopoulos, A. (2021). Methane Cycling within Sea Ice; Results from Drifting Ice during Late spring, north of Svalbard. *The Cryosphere* 15, 2701–2717. doi:10.5194/tc-15-2701-2021
- Wanninkhof, R. (1992). Relationship between Wind Speed and Gas Exchange over the Ocean. *J. Geophys. Res.* 97, 7373–7382. doi:10.1029/92JC00188
- Wegner, C., Wittbrodt, K., Hölemann, J., Janout, M., Kruppen, T., Selyuzhenok, V., et al. (2017). Sediment Entrainment into Sea Ice and Transport in the Transpolar Drift: A Case Study from the Laptev Sea in winter 2011/2012. *Continental Shelf Res.* 141, 1–10. doi:10.1016/j.csr.2017.04.010
- Westbrook, G. K., Thatcher, K. E., Rohling, E. J., Piotrowski, A. M., Pälike, H., and Osborne, A. H. (2009). Escape of Methane Gas from the Seabed along the West Spitsbergen continental Margin. *Geophys. Res. Lett.* 36, L15608. doi:10.1029/2009GL039191
- Wiesenburg, D. A., and Guinasso, N. L. (1979). Equilibrium Solubilities of Methane, Carbon Monoxide, and Hydrogen in Water and Seawater. *J. Chem. Eng. Data* 24, 356–360. doi:10.1021/jc60083a006
- Yamamoto-Kawai, M., Tanaka, N., and Pivovarov, S. (2005). Freshwater and Brine Behaviors in the Arctic Ocean Deduced from Historical Data of $\delta^{18}\text{O}$ and

- Alkalinity (1929-2002 A.D.). *J. Geophys. Res. Ocean.* 110, C10003. doi:10.1029/2004JC002793
- Zhao, M., Timmermans, M.-L., Cole, S., Kishfields, R., Proshutinski, A., and Tolle, J. (2014). Characterizing the Eddies Field in the Arctic Ocean Halocline. *J. Geophys. Res.-Ocean.* 119, 8800–8817. doi:10.1002/2014JC010488
- Zhou, J., Tison, J.-L., Carnat, G. N., Geilfus, X., and Delille, B. (2014). Physical Controls on the Storage of Methane in Landfast Sea Ice. *The Cryosphere* 8, 1019–1029. doi:10.5194/tc-8-1019-2014
- Zhulidov, A. V., and Emetz, V. M. (1991). *Biogeochemical Regionalization of the USSR. Manuscript*. Rostov on Don: Hydrochemical Institute, 625. p. (in Russian).

Conflict of Interest: The authors declare that the research was conducted in the absence of any commercial or financial relationships that could be construed as a potential conflict of interest.

The reviewer TW declared a shared affiliation with the author AP to the handling editor at time of review.

Publisher's Note: All claims expressed in this article are solely those of the authors and do not necessarily represent those of their affiliated organizations, or those of the publisher, the editors and the reviewers. Any product that may be evaluated in this article, or claim that may be made by its manufacturer, is not guaranteed or endorsed by the publisher.

Copyright © 2022 Vinogradova, Damm, Pnyushkov, Krumpfen and Ivanov. This is an open-access article distributed under the terms of the Creative Commons Attribution License (CC BY). The use, distribution or reproduction in other forums is permitted, provided the original author(s) and the copyright owner(s) are credited and that the original publication in this journal is cited, in accordance with accepted academic practice. No use, distribution or reproduction is permitted which does not comply with these terms.